In Vivo Validation of a One-Dimensional Finite-Element Method for Predicting Blood Flow in Cardiovascular Bypass Grafts

Brooke N. Steele*, *Member, IEEE*, Jing Wan, Joy P. Ku, *Member, IEEE*, Thomas J. R. Hughes, and Charles A. Taylor, *Member, IEEE*

***Abstract*—Current practice in vascular surgery utilizes only diagnostic and empirical data to plan treatments and does not enable quantitative *a priori* prediction of the outcomes of interventions. We have previously described a new approach to vascular surgery planning based on solving the governing equations of blood flow in patient-specific models. A one-dimensional finite-element method was used to simulate blood flow in eight porcine thoracothoraco aortic bypass models. The predicted flow rate was compared to *in vivo* data obtained using cine phase-contrast magnetic resonance imaging. The mean absolute difference between computed and measured flow distribution in the stenosed aorta was found to be 4.2% with the maximum difference of 10.6% and a minimum difference of 0.4%. Furthermore, the sensitivity of the flow rate and distribution with respect to stenosis and branch losses were quantified.**

***Index Terms*—Blood flow, one-dimensional analysis methods, simulation-based medical planning.**

I. Introduction

In recent years, significant advances in three-dimensional (3-D) cardiovascular imaging techniques such as computed tomography (CT) and magnetic resonance imaging (MRI) and developments in medical visualization software have provided surgeons with unprecedented tools to examine patient anatomy. Doppler ultrasound and MRI have provided physiologic data to quantify blood flow preoperatively, interoperatively and postoperatively. However, when it comes to surgical planning, all of this data will be put aside as the treatment is sketched using paper and pencil. The surgeon considers the patient's medical condition, expected tolerance to alternate procedures and the anticipated benefit of each treatment based on the outcomes of previous patients with similar conditions. This diagnostic/empirical approach does not enable the *a priori* prediction of the outcomes of alternate interventions for an individual patient, but merely the anticipation that the current patient will have an outcome similar to those of previous patients with similar diagnoses.

We have previously described a new paradigm, predictive medicine, whereby a physician uses a simulation-based medical planning software system in conjunction with patient-specific anatomic and physiologic data to design and preoperatively evaluate treatment plans [1]. For cardiovascular bypass surgery, the ability to predict changes in blood flow would enable a surgeon to evaluate the efficacy of a treatment strategy. In the case where several treatment options exist, the surgeon could use information from simulations to aid in decision-making by ranking treatments based on expected improvement in physiologic function.

Simulations of physiologic function involve solving systems of equations governing blood flow. To date, we have solved the time-dependent, 3-D equations governing blood flow to obtain detailed data on blood flow distribution, wall shear stress, particle residence time and flow recirculation [1]–[5]. However, these 3-D methods are computationally expensive and while important in determining local flow patterns, are not suitable for rapid evaluation of surgical treatments.

Simpler zero- and one-dimensional (1-D) methods have been used to describe blood flow in arteries and quantify mean flow rate and pressure. Zero-dimensional methods or electrical analogs do not define vessel geometry. Instead they represent overall behavior in a collection of vessels by combining resistors and inductors to represent the viscous and inertial properties of blood and capacitors to represent elastic wall behavior. Lumped-parameter methods can be used to represent a single vessel segment or a collection of vessels and have been applied to model blood flow in large portions of the human arterial system [6]–[12]. Electrical analogs are well suited to modeling relations between cardiac output and peripheral load and have significant value as boundary conditions for other analysis methods. However, since geometry is not explicitly defined, wave propagation effects are not modeled. Furthermore, the direct measurement of resistive, inductive and capacitive values for patient specific models is not possible. These values are typically chosen to fit experimental data.

One-dimensional methods are based on the assumption that blood flow velocity along the vessel axis is much greater than flow velocity perpendicular to the vessel axis. Velocity and pressure are averaged over the cross section of the vessel resulting

Manuscript received September 7, 2001; revised October 4, 2002. This work was supported in part by the Whitaker Foundation and in part by the American Heart Association, Western States Affiliate. *Asterisk indicates corresponding author.*

*B. N. Steele is with the Department of Mechanical Engineering, Stanford University, 1201 Welch Road, Room P224, Stanford, CA 94305-5464 USA (e-mail: bnsteele@stanford.edu).

J. Wan is with the Department of Petroleum Engineering, Stanford University, Stanford, CA 94305-5464 USA.

J. P. Ku is with the Department of Electrical Engineering, Stanford University, Stanford, CA 94305-5464 USA.

T. J. R. Hughes is with the Department of Mechanical Engineering, Stanford University, Stanford, CA, 94305-5464 USA.

C. A. Taylor is with the Department of Mechanical Engineering and the Department of Surgery, Stanford University, Stanford, CA, 94305-5464 USA.

Digital Object Identifier 10.1109/TBME.2003.812201

in a coupled system of nonlinear partial differential equations in a single spatial variable and time. Under the assumptions of small perturbations about a zero pressure and axial velocity reference state, a linear form of the equations can be derived. The resultant linear partial differential equations can be solved using Womersley's theory of vascular impedance to model wave propagation in the human arterial system [13], [14]. The linear form of the equations has been used to model wave propagation in the human arterial system [6], under normal and simulated pathological conditions [15], as well as for randomly branched [16] and asymmetric fractal-like models [17]. Impedance-based methods have great utility in describing pressure and flow wave propagation in vessels, but these models do not incorporate nonlinear advective losses or pressure-dependent changes in cross-sectional area [18].

The 1-D nonlinear equations for pulse wave propagation in elastic tubes have been solved using numerical methods to calculate pressure and flow propagation in the human arterial system [18]–[23]. Several of these models have been used to investigate changes in pressure waveforms in an attempt to diagnose disease [18], [21], [22]. The shortcoming of 1-D methods is that they do not account for energy losses associated with secondary flows due to curvature, branching and stenoses. Analytical losses have been added to model the effects of stenoses [24], [25]. Losses associated with vessel curvature and junctions were incorporated by Olufsen *et al.* [23]. While these losses are generally small, in the presence of collateral vessels and bypass grafts they can play a significant role in flow distribution between alternate pathways. Previous studies have not incorporated collateral flow pathways. Accurate modeling of collateral flow is crucial in surgical bypass planning as disease and treatment methods alter blood flow distribution amongst alternate pathways.

To date, only a few investigators have validated their numerical methods with *in vivo* experiments. Holenstein *et al.* used *in vivo* Duplex ultrasound measurements to quantify blood velocity in the superior mesenteric arteries of 35 young, normal individuals for comparison with calculated maximum and minimum flow velocities and flow reversal [8]. Olufsen used MRI data for one subject to validate a novel method for specifying boundary conditions for 1-D methods [23].

We have previously described a finite-element method for solving the 1-D nonlinear equations of blood flow [26]. We have shown that although 1-D analysis methods cannot provide the same level of detail as 3-D methods, they may provide adequate information with which to rank treatment outcomes based on predicted mean flow rate and pressure distribution [26].

This paper describes the experimental validation of a 1-D finite-element analysis technique. A series of animal experiments were performed to test the accuracy of our 1-D methods for modeling blood flow by comparing predicted flow rates to *in vivo* measurements obtained using phase-contrast MRI (PC-MRI) [5]. Thoraco-thoraco bypass surgery was performed on eight pigs to direct blood flow around a surgically induced stenosis. Using a 1-D approximation to the model geometries and flow boundary conditions, we compare the flow rate, mean flow and flow distribution predicted by our 1-D method with experimental data. We demonstrate that a 1-D method incorporating stenosis and branch loss models can adequately describe blood flow distribution in a porcine thoraco-thoraco bypass surgery.

II. Methodology

A. One-Dimensional Method

The 1-D equations for the flow of a Newtonian fluid in an impermeable, deforming, elastic domain consist of the continuity equation, a single axial momentum balance equation, a constitutive equation, and suitable initial and boundary conditions. The governing equations are derived in general form by Hughes and Lubliner [27]. The partial differential equations for mass and momentum balance are given by

$$\frac{\partial S}{\partial t}+\frac{\partial Q}{\partial z}=0 \tag{1}$$

and

$$\frac{\partial Q}{\partial t}+\frac{\partial}{\partial z}\left((1+\delta)\frac{Q^2}{S}\right)+\frac{S}{\rho}\frac{\partial p}{\partial z}=N\frac{Q}{S}+\nu\frac{\partial^2 Q}{\partial z^2}. \tag{2}$$

The primary variables are cross-sectional area S, pressure p and volumetric flow rate Q. The density of the fluid is given by ρ and the kinematic viscosity by ν. The variable δ is related to the profile function for the velocity over the cross-sectional area and N is a viscous loss term. We assume that the axial velocity is much greater than the radial velocity components. If we specify the vessel to have a circular cross section and assume an axisymmetric quadratic flow profile, we obtain

$$\delta=\frac{1}{3} \tag{3}$$

and

$$N=-8\pi\nu. \tag{4}$$

For boundary conditions, we specify the flow rate at the inlet and prescribe a resistance boundary condition at the outlet(s)

$$Q(z,t)=Q(t)\; z\in\Gamma_{\text{in}} \tag{5}$$

$$p\,(z,t)-Q\,(z,t)\,R=0\; z\in\Gamma_{\text{out}}. \tag{6}$$

The initial conditions for this problem are given by

$$S\,(z,0)=S_0\,(z)\,,Q\,(z,0)=Q_0(z). \tag{7}$$

In order to complete the above system, we need to introduce a constitutive relationship. An elastic model is assumed which relates the pressure to the luminal cross-sectional area as follows:

$$p\,(z,t)=\hat{p}\,(S\,(z,t)\,,z,t)\,. \tag{8}$$

We use the constitutive equation described by Olufsen [20]

$$\tilde{p}\,(S(z,t),z,t)=p_0+\frac{4}{3}\frac{Eh}{r_0(z)}\left(1-\sqrt{\frac{S_0(z)}{S(z,t)}}\right) \tag{9}$$

where

$$\frac{Eh}{r_0(z)}=k_1\exp\left[k_2 r_0(z)\right]+k_3. \tag{10}$$

E is the Young's modulus, h is the wall thickness, and r_0 is the radius at the reference pressure p_0. In the relationship, k_1, k_2,

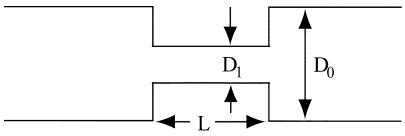

Fig. 1. Stenosis model diagram.

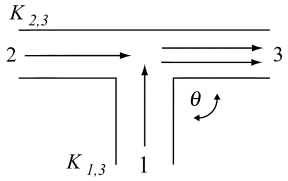

Fig. 2. Converging flow diagram. Loss coefficients are computed for upstream ($K_{2,3}$) and branch ($K_{1,3}$) vessels.

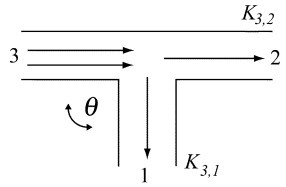

Fig. 3. Diverging flow diagram. Loss coefficients are computed for downstream ($K_{3,2}$) and branch ($K_{3,1}$) vessels.

and k_3 are derived by a best fit to experimental data and are set to default values of $k_1 = 2{\times}10^7\ \mathrm{g{\cdot}s^{-2}{\cdot}cm^{-1}}$, $k_2 = -22.53\ \mathrm{cm^{-1}}$, and $k_3 = 8.65 \times 10^5\ \mathrm{g \cdot s^{-2} \cdot cm^{-1}}$ [20].

To solve the system of equations, we employ a space-time finite-element method including Galerkin Least Squares stabilization in space and the Discontinuous Galerkin method in time. We use a modified Newton–Raphson technique to solve the resultant nonlinear equations for each time step [26].

For the 1-D theory, the assumptions made for the flow profile are not valid in regions of flow separation such as downstream of stenoses or branches and the 1-D method does not adequately model the pressure losses. In fluid systems where vessel lengths are relatively small, losses associated with curvature, branching, valves, contraction, and expansion become important and dominate the overall energy loss of the system. The minor loss coefficient, K [28], is defined as a relationship between fluid density ρ, vessel flow rate Q, cross-sectional area S and the change in pressure Δp

$$K = \frac{\Delta p}{\frac{1}{2}\rho\left(\frac{Q}{S}\right)^2}. \tag{11}$$

We can incorporate the experimentally determined, dimensionless form, K, into our numerical model through the viscous loss term N. Starting with (2) and assuming a constant flow rate, we obtain

$$\frac{1}{\rho}\frac{dp}{dz} = N\frac{Q}{S^2}. \tag{12}$$

If we assume a straight vessel, we can integrate over the length of the vessel and solve for N

$$N = \frac{\Delta p}{\rho}\frac{S^2}{QL}. \tag{13}$$

Combining (11) and (13), we obtain

$$N = \frac{QK}{2L}. \tag{14}$$

We implemented the minor loss value for a stenosis model developed by Seeley and Young [24]. This model utilizes the area ratio between the stenosed segment and the distal normal segment (Fig. 1) to obtain

$$K = 2\left(\frac{K_v}{\mathrm{Re}_0} + \frac{K_t}{2}\left[\frac{S_0}{S_1} - 1\right]^2\right)\left(\frac{S_1}{S_0}\right)^2. \tag{15}$$

Re_0 is the Reynolds number in the unobstructed section, S_0 is the unobstructed cross-sectional area and S_1 is the stenosed cross-sectional area. The coefficient K_v represents viscous losses that dominate at low Reynolds numbers. Experiments show a dependence of K_v on the geometric terms L/D_0 and S_0/S_1 resulting in the predicted equation based on Poiseuille losses

$$K_v = 32\frac{L}{D_0}\left(\frac{S_0}{S_1}\right)^2. \tag{16}$$

This equation is improved by applying a linear Couette correction to L giving

$$K_v = 32\frac{L_a}{D_0}\left(\frac{S_0}{S_1}\right)^2 \tag{17}$$

with

$$L_a = 0.83L + 1.64D_1. \tag{18}$$

The coefficient K_t represents turbulent affects that dominate at high Reynolds numbers. K_t showed little variation with stenosis geometry and is assumed to be independent of geometry. The average value from experimental results gives

$$K_t = 1.52. \tag{19}$$

This stenosis loss coefficient, K, is used in (14) for segments that have clinically significant stenosis of 75% or more decrease in area compared to the distal segment area.

We implemented minor loss values, or junction losses, for branch junctions of arbitrary angles using a model developed by Gardel [29]–[31]. For each branching case of converging flow (Fig. 2) and diverging flow (Fig. 3), minor loss coefficients are computed for the through and branching segment with respect to the combined, or total flow, segment. The branch, through and combined legs are labeled 1, 2, and 3, respectively.

Junction loss coefficients are computed for each through (vessel 2) and branch (vessel 1) segment. The coefficient $K_{1,3}$ is the minor loss coefficient for the converging flow branch leg. The subscripts indicate flow from vessel 1 into vessel 3. The coefficient $K_{2,3}$ is the minor loss coefficient for the through leg of the converging flow case. Similarly, $K_{3,2}$ refers to the minor loss coefficient for the through leg of the diverging flow, flow from vessel 3 into vessel 2 and $K_{3,1}$ refers to the loss

coefficient for the branch leg of the diverging flow case. The coefficients are given as

$$K_{1,3} = 0.92(1+q)^2 + q^2\left[1.2\left(\frac{\cos\theta}{a}-1\right)+0.8\left(1-\frac{1}{a^2}\right) -(1-a)\frac{\cos\theta}{a}\right] + (2-a)q(1+q) \quad (20)$$

$$K_{2,3} = -0.03(1+q)^2 + q^2\left[1+0.62\left(\frac{\cos\theta}{a}-1\right)-0.38(1-a)\right] + (2-a)q(1+q) \quad (21)$$

$$K_{3,1} = -0.95(1-q)^2 - q^2\left[1.3\cot\left(\frac{180-\theta}{2}\right)-0.3+\frac{0.4-0.1a}{a^2}\right] - 0.4q(1-q)\left(1+\frac{1}{a}\right)\cot\frac{180-\theta}{2} \quad (22)$$

$$K_{3,2} = -0.03(1-q)^2 - 0.35q^2 + 0.2q(1-q) \quad (23)$$

where θ is the side branch angle between vessels 1 and 3, q is the flow ratio through the side branch vessel to the combined flow vessel $q = q_1/q_3$ and a is the area ratio of the side branch vessel to the combined branch vessel, $a = a_1/a_3$. The first term in each equation describes the head loss in the through vessel, the second term describes the head loss in the branch vessel and the third term is an additional loss used to match experimental data. These K values are used in (14) for the branch and through segments at junctions. Examples of K value assignments can be seen in Fig. 6.

B. In Vivo Experiment

We used data collected from experiments involving eight pigs. The university's Institutional Animal Care and Use Committee approved all animal procedures. In each animal, we created an aortic constriction, or stenosis, by tying polyester (Dacron) umbilical tape around the descending thoracic aorta to restrict blood flow and create a simulated diseased state. The stenosis ranged from 78% to 93% reduction in the lumen diameter. A 10.0-mm-diameter polyester (Dacron) graft was attached to the thoracic aorta above and below the constriction to provide an alternate path for blood flow. This model resembles the anatomy of patients who have been diagnosed with aorto-iliac disease and have been treated with an aorto-femoral bypass with proximal end-to-side anastomosis. In both cases, blood is divided between the native aorta and the bypass graft above the stenosis and combined downstream of the stenosis.

Anatomic and physiological data was acquired for each animal using MRI. Contrast-enhanced magnetic resonance angiography (CE-MRA) was used to acquire 3-D anatomic images of blood vessels, while phase contrast MRI (PC-MRI) was used to collect velocity information at four different locations: the proximal aorta (inlet), the mid-aorta (aorta), the graft and the distal aorta (outlet) (Fig. 4). Pressure catheters were used to measure the blood pressure proximal and distal to the bypass region [5].

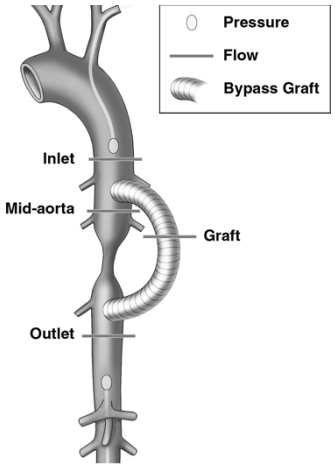

Fig. 4. *In vivo* geometry and PC-MRI acquisition locations for porcine experiments.

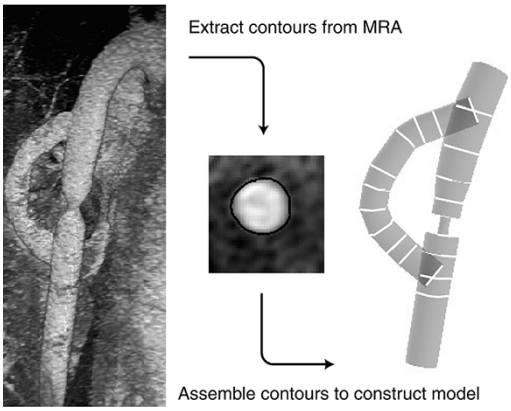

Fig. 5. Model construction process. Reconstruct 3-D geometry from contrast enhanced magnetic resonance angiography data. Extract cross-sectional contours from reconstruction along vessel centerline using level-set method. Create mathematical representation of bypass model with native aorta and bypass graft using the extracted contours.

Using a previously described process [32], a geometric model of the thoracic aorta and corresponding bypass was constructed from the CE-MRA data of each animal. The level set method was used to automatically segment out lumen boundaries of the native aorta and bypass (Fig. 5). For simplicity, the cross-sectional contours of the vessels were approximated with circles and intercostal vessels were not modeled. The contour shape and location are used in the construction of the 1-D models. A velocity profile was generated from the PC-MRI data at the inlet location using custom software [33]. The geometric model, inlet velocity profile and a resistance outlet boundary condition were used to simulate the blood flow for each animal using the 1-D finite-element method previously described.

C. Analysis

All simulations were run on a Silicon Graphics 320 workstation with a Xenon 500 MHz processor and 512 Mb of RAM running Windows NT. A maximum element size of 0.25 cm was used to ensure equally sized elements per vessel segment, with a maximum of 289 and a minimum of 188 elements. The solution was run using 50 time steps per cardiac cycle for three cycles. A resistance of 1440 dynes $\cdot$ s/cm^5, the mean outlet resistance

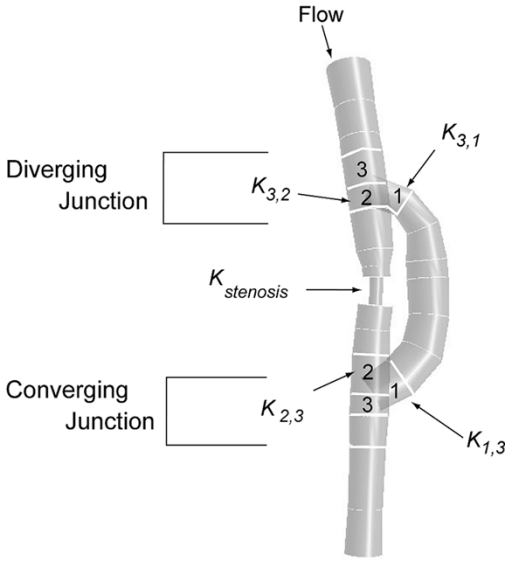

Fig. 6. Model tagging diagram. Junction vessels are numbered and junctions are identified. Subscripts for junction losses indicate direction of flow, from first subscript to second subscript.

measured *in vivo*, was used as the exit boundary condition for all models. Postoperatively measured flow waveforms were used as the inlet boundary conditions for each model.

Each experimental model is composed of an aorta and a graft vessel. Each vessel is comprised of segments that are defined by the cross-sectional profiles segmented from PC-MRI. Each segment, therefore, has a length (distance between consecutive profile slices) and radius. All of the vessel segments, with exception of the stenosis segments, are tapered. The nodes of the stenosed segment are treated like branch points where pressure and flow are continuous but area is not.

Segments are tagged to indicate regions of complex geometry where a minor loss correction should be used. Minor loss tags specify the type of minor loss (stenosis, converging branch segment, converging through segment, diverging branch segment and diverging through segment) as well as information that might be needed in the loss computation. Stenosis segment tags include an identifier for the segment immediately distal to it for use in the calculation of K_{stenosis}. Branch segment tags contain identifiers to the combined segment, branch segment (for through branches) and branch angle for use in the calculations of K_{junction} (Fig. 6). The segments are tagged when the model is read in and after any user specified modifications are made.

III. Results

Mean flow rate was extracted from both the *in vivo* PC-MRI data and the 1-D finite-element method at the inlet, aorta, graft and outlet for each pig in the postoperative, or open bypass graft, configuration. The flow values are plotted for the 1-D analysis and PC-MRI for both the aorta and graft for each pig in Fig. 7. The ratio of mean flow for the aorta and graft to the total flow is shown in Fig. 8.

We study the effects of loss terms by comparing blood flow rate with and without junction losses. We choose an example where final computed results compare well with experimental data and compare the effect of including both stenosis and junction loss terms with only stenosis losses (Fig. 9). The aortic flow ratio without the junction loss term is 0.029, significantly lower than the mean predicted flow ratio with the junction loss term of 0.108 and the measured aortic flow ratio, 0.153.

IV. Discussion

While the 1-D model does not exactly match the PC-MRI data, it does provide a good approximation to the flow rate distribution between the aorta and bypass. Considering the ratio of total flow through the aorta, the average difference between predicted and measured flow ratio is 4.8% with the maximum difference of 10.6% and a minimum difference of 0.4%. Only one of the eight predictions shows a difference of greater than 10%. There are a few possible sources for the differences observed.

First, the empirical methods used to model energy loss for complex geometry were developed under steady flow conditions for rigid vessels and may not be optimal for use in deformable vessels with pulsatile flow. A pulsatile model has been described for stenosis loss and will be evaluated in future work [25]. Losses associated with curvature are not included. In Fig. 9 we see the effect of the junction loss coefficients. The junction loss models are defined to have one straight through leg and one branch leg. Future work will include determining the appropriate junction loss coefficients to use for a bifurcating vessel.

Second, there are measurement errors associated with the experimental protocol and the PC-MRI method for measuring blood flow velocity. A potential source of error could be due to physiological changes in the pigs during the time required to complete all PC-MRI scan sequences. While every effort was made to keep the physiological state of the pigs constant during the time it took to acquire all of the flow velocity scans, some variations may have occurred. There may also have been variability in velocity data acquisition and extraction from PC-MRI. Combinations of these and other errors may account for phase shift of the curves and the fact that experimentally measured flow is not precisely conserved in our region of interest. When the mean flow ratios were computed with respect to the combined flow between the aorta and graft, the 1-D and PC-MRI values compared favorably (Fig. 7). With 10.59% difference between the predicted and computed flow ratios, the predicted flow distribution for pig C does not agree as well as in the other experiments. For all pigs except C, a two-dimensional (2-D) segmented k-space MR sequence [34]–[36] was used to acquire the velocity component along the axis of the vessel. Respiration was suspended for these scans. For pig C, a 2-D cine phase contrast sequence [37], [38] was used to obtain three orthogonal components of velocity. Respiration was not suspended for this scan.

Third, the accuracy of the model geometry is limited by the CE-MRA resolution. Each pixel ranges in size from 0.46 mm to 0.63 mm. The radii of the stenoses range from approximately 2.49 to 1.38 mm. An error of one half of a pixel on either side of the vessel in the stenosis region could distort the results. An example of this can be seen with pig E where the minimum stenosis radii obtained using our segmentation method was 1.38 mm. We examined the effect of a radius corresponding to one half of a pixel larger, or 1.68 mm. Improvements in the

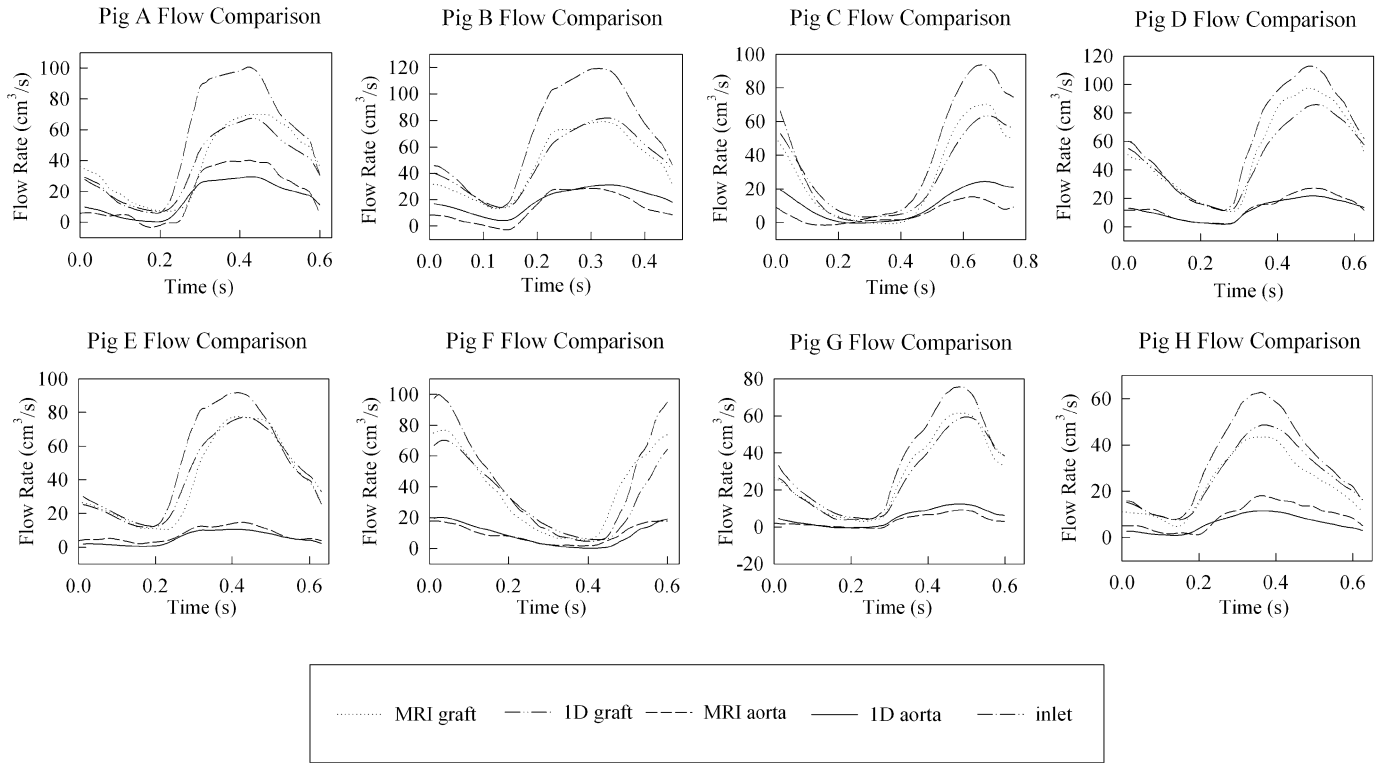

Fig. 7. Mean flow taken at inlet, graft and aorta of the *in vivo* experiments and 1-D models.

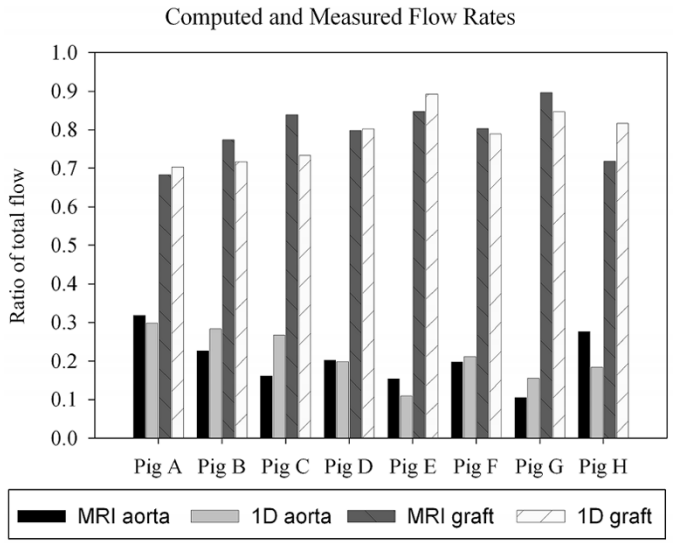

Fig. 8. Computed and measured flow ratios of blood flow through the native aorta to total flow and bypass graft to total flow.

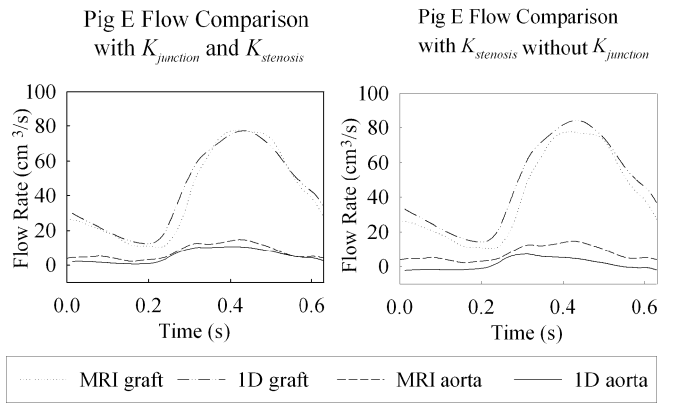

Fig. 9. Effect of junction loss on mean flow distribution. Without junction loss, flow through bypass graft is overestimated.

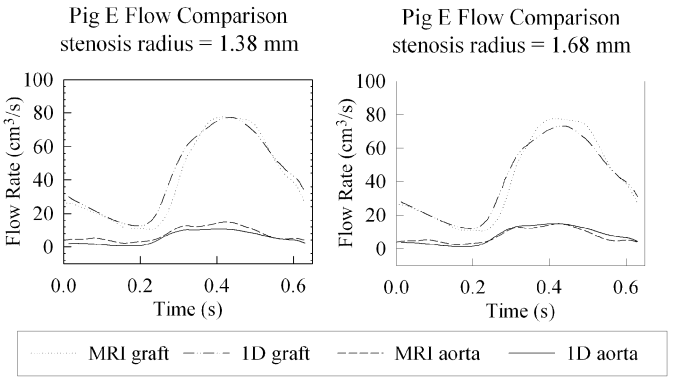

Fig. 10. Sensitivity of flow distribution to stenosis radius. Flow ratio through aorta increases 44% when stenosis radius is increased 22% from 1.38 mm to 1.68 mm (one half of an image pixel).

correlation between computed and measured flow rate were observed as shown in Fig. 10. The predicted flow ratio through the aorta increases from 0.11 to 0.16, a value more comparable with the measured ratio of 0.15.

Fourth, the boundary condition used for all pigs was an average based on pressure and flow measurements in several pigs. Although the resistance boundary condition may give rise to artificial pulse wave reflections, this boundary condition was relatively easy to implement in our finite-element method. The results show that even with this boundary condition flow rate and

distribution can be predicted accurately. Future work will investigate the use of alternate boundary conditions.

Further validation studies are needed to predict postoperative blood flow based on preoperative data. For this experiment we were able to specify the inlet boundary conditions for each model using the postoperatively measured volume flow. This data would not be available in a true planning scenario. Future work will include developing methods for determining postoperative inlet boundary conditions from preoperative data.

V. Conclusion

We have demonstrated that a 1-D finite-element method can be used to predict the flow distribution in a cardiovascular bypass graft. Numerical predictions of flow rate were compared with MRI data in eight pigs. Less than 11% error was observed in the flow ratios of all eight animals. It was shown that for this analysis of blood flow through a bypass graft, it was necessary to include the effects of junction losses in addition to stenosis losses.

Acknowledgment

The authors acknowledge the assistance of F. Arko, M. Draney, W. A. Lee, F. Chan, N. Pelc, C. Zarins, D. Howard, A. Sawyer-Glover, W. Baumgardner, T. Brosnan, K. Wang and N. Wilson.

References

[1] C. A. Taylor, M. T. Draney, J. P. Ku, D. Parker, B. N. Steele, K. Wang, and C. K. Zarins, "Predictive medicine: Computational techniques in therapeutic decision-making," *Comput. Aided Surg.*, vol. 4, pp. 231–247, 1999.

[2] C. A. Taylor, T. J. R. Hughes, and C. K. Zarins, "Finite element modeling of blood flow in arteries," *Comput. Meth. Appl. Mech. Eng.*, vol. 158, pp. 155–196, 1998.

[3] ——, "Finite element modeling of three-dimensional pulsatile flow in the abdominal aorta: Relevance to atherosclerosis," *Ann. Biomed. Eng.*, vol. 26, pp. 1–14, 1998.

[4] ——, "Effect of exercise on hemodynamic conditions in the abdominal aorta," *J. Vasc. Surg.*, vol. 29, pp. 1077–1089, 1999.

[5] J. P. Ku, M. T. Draney, F. R. Arko, W. A. Lee, F. P. Chan, N. J. Pelc, C. K. Zarins, and C. A. Taylor, "*In vivo* validation of numerical prediction of blood flow in arterial bypass grafts," *Ann. Biomed. Eng.*, vol. 30, pp. 743–752, 2002.

[6] N. Westerhof, F. Bosman, C. J. De Vries, and A. Noordergraaf, "Analog studies of the human systemic arterial tree," *J. Biomech.*, vol. 2, pp. 121–143, 1969.

[7] L. Pater and J. W. v. d. Berg, "An electrical analogue of the entire human circulatory system," *Med. Electron. Biol. Eng.*, vol. 2, pp. 161–166, 1964.

[8] R. Holenstein and D. N. Ku, "Reverse flow in the major infrarenal vessels—A capacitive phenomenon," *Biorheology*, vol. 25, pp. 835–842, 1988.

[9] R. Pietrabissa, S. Mantero, T. Marotta, and L. Menicanti, "A lumped parameter model to evaluate the fluid dynamics of different coronary bypasses," *Med. Eng. Phys.*, vol. 18, pp. 477–484, 1996.

[10] T. S. Manning, B. E. Shykoff, and J. L. Izzo Jr., "Validity and reliability of diastolic pulse contour analysis (windkessel model) in humans," *Hypertension*, vol. 39, pp. 963–968, 2002.

[11] E. B. Shimm, R. D. Kamm, T. Heldt, and R. G. Mark, "Numerical analysis of blood flow through a stenosed artery using a coupled, multiscale simulation method," *Comput. Cardiol.*, vol. 27, pp. 219–222, 200.

[12] R. W. Eckstein, D. E. Gregg, and W. H. Pritchard, "The magnitude ant time of development of the collateral circulation in occluded femoral, carotid and coronary arteries," *Amer. J. Physiol.*, vol. 132, pp. 351–361, 1940.

[13] M. G. Taylor, "The input impedance of an assembly of randomly branching elastic tubes," *Biophys. J.*, vol. 6, pp. 29–51, 1966.

[14] J. R. Womersley, "Oscillatory motion of a viscous liquid in a thin-walled elastic tube—I: The linear approximation for long waves," *Philosophical Mag.*, vol. 7, pp. 199–221, 1955.

[15] A. P. Avolio, "Multi-branched model of the human arterial system," *Med. Biol. Eng. Comput.*, vol. 18, pp. 709–718, 1980.

[16] M. G. Taylor, "Wave transmission through an assembly of randomly branching elastic tubes," *Biophys. J.*, vol. 6, pp. 697–716, 1966.

[17] D. J. Brown, "Input impedance and reflection coefficient in fractal-like models of asymmetrically branching compliant tubes," *IEEE Trans. Biomed. Eng.*, vol. 43, pp. 715–722, July 1996.

[18] J. K. Raines, M. Y. Jaffrin, and A. H. Shapiro, "A computer simulation of arterial dynamics in the human leg," *J. Biomech.*, vol. 7, pp. 77–91, 1974.

[19] N. Stergiopulos, D. F. Young, and T. R. Rogge, "Computer simulation of arterial flow with applications to arterial and aortic stenoses," *J. Biomech.*, vol. 25, pp. 1477–1488, 1992.

[20] M. S. Olufsen, "A structured tree outflow condition for blood flow in the larger systemic arteries," *Amer. J. Physiol.*, vol. 276, pp. H257–H268, 1999.

[21] B. Hillen, H. W. Hoogstraten, and L. Post, "A mathematical model of the flow in the circle of willis," *J. Biomech.*, vol. 19, pp. 187–194, 1986.

[22] S. D. Balar, T. R. Rogge, and D. F. Young, "Computer simulation of blood flow in the human arm," *J. Biomech.*, vol. 22, pp. 691–697, 1989.

[23] M. S. Olufsen, C. S. Peskin, W. Y. Kim, E. M. Pedersen, A. Nadim, and J. Larsen, "Numerical simulation and experimental validation of blood flow in arteries with structured-tree outflow conditions," *Ann. Biomed. Eng.*, vol. 28, pp. 1281–1299, 2000.

[24] B. D. Seeley and D. F. Young, "Effect of geometry on pressure losses across models of arterial stenoses," *J. Biomech.*, vol. 9, pp. 439–448, 1976.

[25] D. F. Young and F. Y. Tsai, "Flow characteristics in models of arterial stenoses. II. Unsteady flow," *J. Biomech.*, vol. 6, pp. 547–559, 1973.

[26] J. Wan, B. N. Steele, S. Spicer, S. Strohband, G. Feijoo, T. J. R. Hughes, and C. A. Taylor, "A one-dimensional finite element method for simulation-based medical planning for cardiovascular disease," *Comput. Meth. Biomech. Biomed. Eng.*, vol. 5, pp. 195–206, 2002.

[27] T. J. R. Hughes and J. Lubliner, "On the one-dimensional theory of blood flow in the larger vessels," *Math. Biosci.*, vol. 18, pp. 161–170, 1973.

[28] B. R. Munsun, D. F. Young, and T. H. Okiishi, "Viscous flow in pipes," in *Fundamentals of Fluid Mechanics*. New York: Wiley, 1990, pp. 504–517.

[29] D. J. Wood, L. S. Reddy, and J. E. Funk, "Modeling pipe networks dominated by junctions," *J. Hydraulic Eng.*, vol. 119, pp. 949–958, 1993.

[30] A. Gardel, "Les pertes de charge dans les écoulements au travers de branchments en té," *Bull. Technique de la Suisse Romande*, vol. 10, pp. 143–148, 1957.

[31] ——, "Les pertes de charge dans les écoulements au traverse de branchments en té," *Bull. Technique de la Suisse Romande*, vol. 9, pp. 123–130, 1957.

[32] K. C. Wang, R. W. Dutton, and C. A. Taylor, "Level sets for vascular model construction in computational hemodynamics," *IEEE Eng. Med. Biol.., Mag.*, vol. 18, pp. 33–39, 1999.

[33] N. J. Pelc, F. G. Sommer, K. C. P. Li, T. J. Brosnan, R. J. Herfkens, and D. R. Enzmann, "Quantitative magnetic resonance flow imaging," *Magn. Reson. Quart.*, vol. 10, pp. 125–147, 1994.

[34] J. O. Fredrickson and N. J. Pelc, "Time resolved MR imaging by automatic data segmentation," *J. Magn. Reson. Imag.*, vol. 4, pp. 189–196, 1994.

[35] C. Thomsen, M. Corsten, L. Sondergaard, O. Henriskon, and F. Stahlberg, "A segmental k-space velocity mapping protocol for quantification of renal artery blood flow during breath-holding," *J. Magn. Reson. Imag.*, vol. 5, pp. 393–401, 1995.

[36] M. H. Buonocore, L. Gao, and H. G. Bogren, "Experimental study of the effects of fractional gating on flow measurements," *J. Magn. Reson. Imag.*, vol. 2, p. 142, 1992.

[37] G. L. Nayler, D. N. Firmin, and D. B. Longmore, "Blood flow imaging by cine magnetic resonance," *J. Comput. Assist. Tomogr.*, vol. 10, pp. 715–722, 1986.

[38] N. J. Pelc, R. J. Herfkens, A. Shimakawa, and D. R. Enzmann, "Phase contrast cine magnetic resonance imaging," *Magn. Reson. Quart.*, vol. 7, pp. 229–254, 1991.

Brooke N. Steele (M'01) received the bachelors degree in mechanical engineering from the Georgia Institute of Technology, Atlanta, in 1995 and the masters degree in mechanical engineering with an emphasis on mechatronics design from Stanford University, Stanford, CA, in 1997. She is now working towards the Ph.D. degree in mechanical engineering with an emphasis on biomechanics at Stanford University.

Jing Wan received the B.S. degree in applied mechanics and mechanical engineering from the University of Science and Technology of China, Anhui, China, in 1996 and the M.S. degree in petroleum engineering from Stanford University, Stanford, CA, in 1998. She is currently working towards the Ph.D. degree in petroleum engineering at Stanford University.

Joy P. Ku (M'96) received the B.S. degree in electrical engineering with an emphasis on bioelectronics from the University of California at Berkeley, Berkeley, in 1993 and the M.S. degree in electrical engineering from Stanford University, Stanford, CA, in 1998. She is working towards the Ph.D. degree in electrical engineering at Stanford University.

Her research focuses on the validation of numerical methods for computational fluid dynamics using magnetic resonance imaging techniques.

Ms. Ku has been a recipient of the Hewlett-Packard Resident Fellowship and the American Heart Association, Western States Affiliate's Predoctoral Fellowship.

Thomas J. R. Hughes received the B.S. and M.S. degrees in mechanical engineering from the Pratt Institute, Brooklyn, NY, in 1965 and 1967, respectively, and the M.S. degree in mathematics and the Ph.D. degree in engineering science from the University of California, Berkeley, in 1974.

He is currently Professor of Aerospace Engineering and Engineering Mechanics at the University of Texas at Austin where he occupies the Computational and Applied Mathematics Chair III. Previously, he was the Mary and Gordon Crary Professor of Engineering at Stanford University. He has also taught at the California Institute of Technology and the University of California, Berkeley and he has held industrial positions at Grumman Aerospace and General Dynamics. He is the author of *The Finite Element Method* (Englewood Cliffs, NJ: Prentice-Hall, 1987) (reprinted by New York: Dover, 2000), co-author of *The Mathematical Foundations of Elasticity* (Englewood Cliffs, NJ: Prentice-Hall, 1983), (reprinted by New York: Dover, 1994) and *Computational Inelasticity* (Berlin, Germany: Springer-Verlag, 1998).

Professor Hughes is a Fellow of the American Academy of Mechanics, the American Society of Mechanical Engineers (ASME) and the American Association for the Advancement of Science, co-editor of the international journal Computer Methods in Applied Mechanics, a Founder, Fellow and past President of the U.S. Association for Computational Mechanics (USACM) and a Founder, Fellow and past President of the International Association for Computational Mechanics (IACM). He is also a past Chairman of the Applied Mechanics Division of ASME. He has received numerous awards, including the Huber Prize of the American Society of Engineers, the Melville and Warner Medals from ASME, the Von Neumann Medal from USACM and the Gauss-Newton Medal from IACM. He is a member of the National Academy of Engineering.

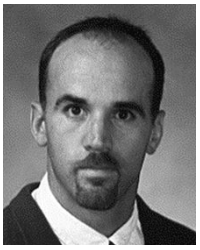

Charles A. Taylor (M'02) received the B.S. degree in mechanical engineering from Rensselaer Polytechnic Institute, Troy, NY, in 1987. He then joined the Engineering Physics Laboratory at GE Research & Development Center in Schenectady, NY, where he worked on projects ranging from polymer process modeling to aircraft engine design. He received the M.S. degree in mechanical engineering and in mathematics from Rensselaer Polytechnic Institute in 1991 and 1992, respectively. He entered the Ph.D. degree program in the Division of Applied Mechanics at Stanford University, Stanford, CA, in 1992 and received the Ph.D. degree in 1996 for his work on finite element modeling of blood flow.

He joined the faculty at Stanford University in 1997 and is currently an Assistant Professor in the Departments of Mechanical Engineering, Surgery and Pediatrics (by courtesy). He founded and directs the Stanford Cardiovascular Biomechanics Laboratory and is particularly interested in the application of computational and advanced imaging methods to the study of the cardiovascular system with applications in disease research, device design and surgery planning. He is a James F. Clark Fellow in Bioengineering at Stanford.

Prof. Taylor received the "Young Investigator in Computational Mechanics Award" in 2002 from the International Association for Computational Mechanics. He is a Member of the American Society of Mechanical Engineers (ASME), the Society for Industrial and Applied Mathematics, the American Mathematical Society, the Biomedical Engineering Society, and the International Society for Magnetic Resonance in Medicine.